Modeling of surface roughness scattering in nanowires based on atomistic wave function: Application to hole mobility in rectangular germanium nanowires

Hajime Tanaka,* Jun Suda, and Tsunenobu Kimoto
Department of Electronic Science and Engineering, Kyoto University, Kyoto 615-8510, Japan
(Received 1 October 2015; revised manuscript received 21 February 2016; published 7 April 2016)

The authors present a calculation model of surface roughness scattering (SRS) in nanowires (NWs) based on atomistic description of electronic states by an $sp^3d^5s^*$ tight-binding scheme, and then this model is applied to hole transport in rectangular cross-sectional germanium (Ge) NWs. In this SRS model, the change of electronic band structures due to width or height reduction is first computed, and then it is expressed using an equivalent potential near the surface. The perturbation corresponding to a surface roughness is calculated from this equivalent potential. Using the aforementioned SRS model, hole mobility in Ge NWs was computed taking into account phonon scattering and SRS. The impacts of SRS on hole mobility in Ge NWs were analyzed, focusing on the valence band structure and hole states of NWs. The main results are as follows. At low hole density, the impacts of SRS are strongly dependent on NW geometry, and Ge NWs with high phonon-limited hole mobility, such as rectangular cross-sectional [110]-oriented NWs with large height along the [001] direction and square cross-sectional [111]-oriented NWs, tend to be less affected by SRS. At high hole density, however, the geometry dependence of hole mobility becomes weaker. These are understood from the nature of hole states and the valence band structure.

DOI: 10.1103/PhysRevB.93.155303

I. INTRODUCTION

Semiconductor nanowires (NWs) are a promising candidate as a channel material of future metal-oxide-semiconductor field-effect transistors (MOSFETs) owing to their high electrostatic controllability and resulting excellent immunity to short-channel effects [1–4]. In particular, germanium (Ge) NWs are attracting a great deal of attention as a p-channel material because of the high hole mobility of Ge [5,6]. For these reasons, a lot of theoretical [7–11] and experimental [12–14] studies on carrier transport in Ge NWs have been reported. Previous studies on hole transport properties in Ge NWs predict that higher phonon-limited hole mobility than in bulk Ge may be achieved in thin (cross-sectional size of several nanometers) Ge NWs with proper geometries [15,16].

However, carriers in thin NWs, where carriers have large confinement-induced energy, suffer strong surface roughness scattering (SRS) due to large fluctuation of confinement-induced energy [17–19]. For example, holes in Ge NWs can suffer an energy change of a few tens of meV due to height fluctuation of one bilayer when the NW height is 2 nm. To our knowledge, existing theoretical studies on hole mobility in Ge NWs are limited to phonon-limited mobility, which corresponds to the mobility in NWs without imperfections such as surface roughness. To investigate the potential of Ge NWs as a p-channel material in realistic devices with surface roughness, analyzing the impacts of SRS on hole mobility in Ge NWs is important.

SRS in NWs has been studied by various authors using various models [19–22]. Here, we focus on perturbative models, which are suitable for mobility calculation [23]. Jin *et al.* [19] developed an SRS model for circular cross-sectional NWs in the framework of an effective mass approximation. In the same way as their SRS model for ultrathin-body MOSFETs [24], their model for NWs is an extension of Ando's SRS model [25] being valid for bulk MOSFETs. Their models are based on the "generalized Prange-Nee term," which reduces to the Prange-Nee term [26] when carriers are confined by an infinitely high potential barrier, and also consider the roughness-induced Coulomb scattering potential [24]. SRS models based on effective mass approximation are extended to NWs with square and rectangular cross sections [27,28]. As an SRS model with more sophisticated description of electronic states, pseudopotential-based modeling of SRS was reported and applied to silicon NWs [23]. Recently, another SRS model, that can take into account the band anisotropy by using anisotropic effective mass [29,30] or $k \cdot p$ theory [31], was presented for arbitrarily shaped structures including NWs. This model is based on an extension of the Prange-Nee term to nonplaner structures.

On the other hand, SRS models in NWs based on the tight-binding approximation, which describes electrons atomistically and is suitable for nanostructures, have also been reported [32–35]. However, these models treat surface roughness as one-dimensional (along the transport direction) fluctuation of cross-sectional shape of NWs [32–34], or require interpolation of the tight-binding wave function in order to use the expression derived for the continuum wave function [35]. Since atomistic calculations of phonon-limited carrier mobility in NWs using the tight-binding approximation for electrons and the valence force field model for phonons are a timely issue [11,15,16,36–41], a more accurate and useful SRS model for NWs that can be combined with atomistic treatment of phonon scattering is beneficial to extend such atomistic calculation of phonon-limited mobility to SRS.

In this paper, we developed an SRS model suitable for a tight-binding description of electronic states. In this model, we first compute the electronic band structures when the width or height of a NW is slightly reduced. Next the change of E-k dispersion due to size reduction is converted to an equivalent potential near the surface. Using this potential, the

*tanaka@semicon.kuee.kyoto-u.ac.jp

 ©2016 American Physical Society

perturbation corresponding to surface roughness is calculated. Scattering probability is computed by Fermi's golden rule, taking into account the tight-binding wave function and two-dimensional surface roughness. Then, we applied this model to a calculation of the hole mobility in rectangular cross-sectional Ge NWs considering phonon scattering and SRS. The considered orientations and sidewalls of Ge NWs are [001]/(010)/(100), [110]/(1$\bar{1}$0)/(001), [111]/(1$\bar{1}$0)/($\bar{1}\bar{1}$2), and [112]/(1$\bar{1}$0)/($\bar{1}\bar{1}$1), and the cross sections are rectangles with 4 nm width and varied height from 2 to 10 nm. The impacts of SRS on hole mobility were investigated at both low and high hole density, and the effects of NW geometry, hole density, and gate electric field were analyzed.

This paper is organized as follows. Section II explains the developed model of SRS in NWs and the calculation method of mobility. In Sec. III, the calculated hole mobility in Ge NWs is shown, and its geometry and hole density dependencies are presented. The physical understanding of their behavior is discussed. The paper is concluded in Sec. IV.

II. CALCULATION METHODS

A. Modeling of surface roughness scattering

Here, we describe the model of SRS developed in this work. This model is suitable for a tight-binding description of electronic states, but it can be applied to other models for electronic states.

In this model, the effect of surface roughness on electronic states is expressed by an equivalent potential near the surface (equivalent surface roughness potential, V_{ESR}) as in Fig. 1, and the scattering by the corresponding perturbation is formulated by Fermi's golden rule. By introducing V_{ESR}, the two-dimensionality of surface roughness can be taken into account perturbatively without interpolating the wave function. Here, the derivation of the matrix element of the perturbation Hamiltonian is explained. The roughness on the four faces of a rectangular cross-sectional NW was assumed to be uncorrelated, and the total SRS probability was calculated as the sum of the scattering probabilities by each surface, which means that the corners are included in the calculations corresponding to the two neighboring faces. Therefore, the matrix element due to the surface roughness on one sidewall is discussed below.

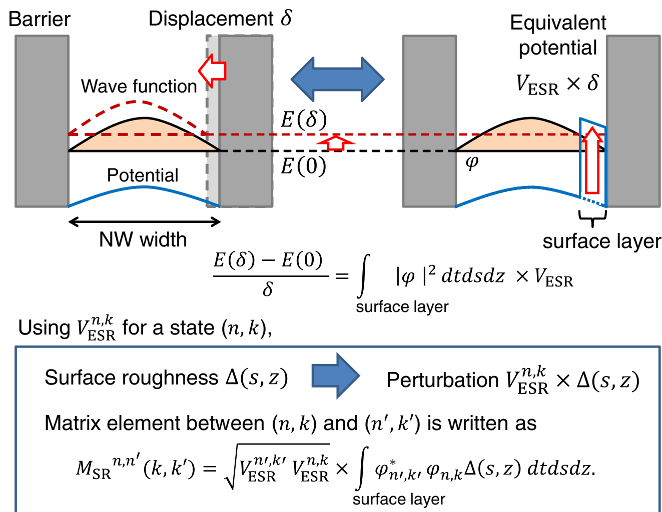

FIG. 1. Schematic image of the SRS model presented in this work. First, the energy variation of subbands due to a small displacement of a sidewall was computed numerically, and this was converted to an equivalent potential applied to thin layers near the sidewall. Then the matrix element corresponding to the perturbation by surface roughness is calculated using this potential energy.

First, the variation of subband structure (E-k dispersion) due to displacement of a sidewall by a small distance δ, $E_{n,k}(\delta) - E_{n,k}(0)$, was calculated for each electronic state (n,k). Here, n and k indicate the subband index and wavenumber, respectively. E-k dispersions were calculated with surface dangling bonds passivated by giving an excess energy to the corresponding sp^3 hybridized orbitals [42]. The small displacement δ is two atomic layers, in order to keep the parity of the total layer number, and the E-k dispersion $E_{n,k}(\delta)$ was calculated by eliminating two atomic layers from the considered structure. Then, we define the sum of probability density of this state (n,k) in the N_{layer} atomic layers near the surface as

$$P^{n,k}_{\text{surface layer}} = \int_{\text{surface}} \left[\int_{\text{layer}} \left| \frac{e^{ikz}}{\sqrt{N_{\text{cell}}}} u_{n,k} \right|^2 dt \right] ds\, dz. \quad (1)$$

Here, z and s denote the position along the transport axis and the perimeter, respectively. $\int_{\text{layer}} dt$ is the integration along the depth direction for N_{layer} atomic layers from the surface. This integration means the summation of tight-binding coefficients belonging to the atoms in the N_{layer} atomic layers in the tight-binding picture. The tight-binding Bloch function $e^{ikz}u_{n,k}$ is normalized in each unit cell with the length L_{cell}, and $\frac{e^{ikz}}{\sqrt{N_{\text{cell}}}}u_{n,k}$ is normalized in the whole system with N_{cell} unit cells, whose length is $L = L_{\text{cell}} \times N_{\text{cell}}$. Using the aforementioned quantities, the equivalent surface roughness potential for (n,k), $V^{n,k}_{\mathrm{ESR}}$, is given as

$$V^{n,k}_{\mathrm{ESR}} = \frac{E_{n,k}(\delta) - E_{n,k}(0)}{\delta} \frac{1}{P^{n,k}_{\text{surface layer}}}. \quad (2)$$

$\delta \times V^{n,k}_{\mathrm{ESR}}$ reproduces the energy variation due to the uniform displacement of a sidewall by δ, as a first-order perturbation potential applied to the N_{layer} atomic layers near the surface. The normalization by $P^{n,k}_{\text{surface layer}}$ in the denominator is required to balance with the probability density in the N_{layer} atomic layers to which the potential is applied. N_{layer} should not be too small because the results should not be affected by the delicate electronic states near the surface. At the same time, it should not be too large in order to avoid the phase variation of wave function along the depth direction. Thus N_{layer} is chosen as 4.

Then, when we define the displacement of interface at a position (s,z) as $\Delta(s,z)$, the corresponding perturbation for a state (n,k) is expressed by a potential $V^{n,k}_{\mathrm{ESR}} \times \Delta(s,z)$ applied on N_{layer} atomic layers near the surface. The sign of $\Delta(s,z)$ (whether the displacement is inward or outward) is reflected in the sign of the potential. The diagonal matrix element of this perturbation for a uniform displacement [$\Delta = \delta$ independently of (s,z)] reproduces the energy shift caused by the same

displacement of a sidewall:

$$M_{\mathrm{SR}}^{n,n}(k,k) = P_{\text{surface layer}}^{n,k} \times V_{\mathrm{ESR}}^{n,k}\delta = E_{n,k}(\delta) - E_{n,k}(0). \quad (3)$$

This validates the definition of Eq. (2), especially the normalization by $P_{\text{surface layer}}^{n,k}$, which may seem counterintuitive. The nondiagonal element between states (n,k) and (n',k') is written as $\sqrt{V_{\mathrm{ESR}}^{n',k'} V_{\mathrm{ESR}}^{n,k}} \times \Delta(s,z)$, assuming the form of a product of factors originating from both states (n,k) and (n',k'), as well as the Prange-Nee term [24–26]. The resulting matrix element for scattering is, by summing up the contribution from each position (s,z),

$$M_{\mathrm{SR}}^{n,n'}(k,k') = \int_{\text{surface}} \left[\int_{\text{layer}} \left(\frac{e^{-ik'z}}{\sqrt{N_{\text{cell}}}} u_{n',k'}^{*} \frac{e^{ikz}}{\sqrt{N_{\text{cell}}}} u_{n,k} \right) dt \times \sqrt{V_{\mathrm{ESR}}^{n',k'} V_{\mathrm{ESR}}^{n,k}}\, \Delta(s,z) \right] ds\, dz. \quad (4)$$

The integral over position means the sum of atomic orbitals in the case of tight binding considered here. The expression of the matrix element in a real-space formalism, which may serve to bridge the real-space treatment of surface roughness based on the nonequilibrium Green's function formalism [20,21] and perturbative approaches, distinguishes our model from previously reported atomistic modelings of surface roughness scattering such as Ref. [23].

To compute the scattering probability from an initial state (n,k) to a final state (n',k') by Fermi's golden rule,

$$S^{n,n'}(k,k') = \frac{2\pi}{\hbar} \langle |M_{\mathrm{SR}}^{n,n'}(k,k')|^2 \rangle \delta(E_{n',k'} - E_{n,k}), \quad (5)$$

we need the squared matrix element averaged over stochastic surface roughness $\langle |M_{\mathrm{SR}}^{n,n'}(k,k')|^2 \rangle$. Defining the local product of the periodic part of Bloch function at (s,z) as

$$\left[\int_{\text{layer}} u_{n',k'}^{*} u_{n,k} dt \right] = D_{\text{layer}}^{k,n,k',n'}(s,z), \quad (6)$$

we have

$$\begin{aligned}
\langle |M_{\mathrm{SR}}^{n,n'}(k,k')|^2 \rangle &= |V_{\mathrm{ESR}}^{n',k'} V_{\mathrm{ESR}}^{n,k}| \left\langle \left| \int_{\text{surface}} \left[\int_{\text{layer}} u_{n',k'}^{*} u_{n,k} dt \right] \frac{e^{i(k-k')z}}{N_{\text{cell}}} \Delta(s,z)\, ds\, dz \right|^2 \right\rangle \\
&= |V_{\mathrm{ESR}}^{n',k'} V_{\mathrm{ESR}}^{n,k}| \left\langle \int_{\text{surface}} D_{\text{layer}}^{k,n,k',n'}(s,z) \frac{e^{i(k-k')z}}{N_{\text{cell}}} \Delta(s,z)\, ds dz \int_{\text{surface}} D^{*k,n,k',n'}_{\text{layer}}(s',z') \frac{e^{-i(k-k')z'}}{N_{\text{cell}}} \Delta(s',z')\, ds' dz' \right\rangle \\
&= |V_{\mathrm{ESR}}^{n',k'} V_{\mathrm{ESR}}^{n,k}| \int_{\text{surface}} \int_{\text{surface}} D_{\text{layer}}^{k,n,k',n'}(s,z) D^{*k,n,k',n'}_{\text{layer}}(s',z') \frac{e^{i(k-k')(z-z')}}{N_{\text{cell}}^2} \langle \Delta(s,z)\Delta(s',z') \rangle\, ds\, dz\, ds' dz', \quad (7)
\end{aligned}$$

which is similar to Eq. (4) in Ref. [29] except for the coefficient. Here, we describe the surface roughness by a correlation function of exponential type [43] with correlation length λ_c and root mean square (RMS) roughness amplitude Δ_{rms} as

$$\langle \Delta(s,z)\Delta(s',z') \rangle = \langle \Delta(0,0)\Delta(s'-s,z'-z) \rangle = \Delta_{\text{rms}}^2 e^{-\sqrt{2}\sqrt{(s'-s)^2+(z'-z)^2}/\lambda_c}. \quad (8)$$

Then, in the integration over the whole surface, the integral along the transport direction z is split into an integral within each unit cell j (length of L_{cell}) at position $z = Z_j$ and a summation over unit cells (N_{cell} cells):

$$\int_{\text{surface}} ds\, dz = \int_{\text{peri}} ds \int_{L=L_{\text{cell}}\times N_{\text{cell}}} dz = \int_{\text{peri}} ds \sum_{j=1}^{N_{\text{cell}}} \int_{L_{\text{cell}}} dz \quad (9)$$

By using the expressions above, we obtain from Eq. (7)

$$\begin{aligned}
&|V_{\mathrm{ESR}}^{n',k'} V_{\mathrm{ESR}}^{n,k}| \int_{\text{surface}} \int_{\text{surface}} D_{\text{layer}}^{k,n,k',n'}(s,z) D^{*k,n,k',n'}_{\text{layer}}(s',z') \frac{e^{i(k-k')(z-z')}}{N_{\text{cell}}^2} \Delta_{\text{rms}}^2 e^{-\sqrt{2}\sqrt{(s'-s)^2+(z'-z)^2}/\lambda_c}\, ds\, dz\, ds' dz' \\
&= |V_{\mathrm{ESR}}^{n',k'} V_{\mathrm{ESR}}^{n,k}| \sum_{j'=1}^{N_{\text{cell}}} \int_{L_{\text{cell}}} \sum_{j=1}^{N_{\text{cell}}} \int_{L_{\text{cell}}} \int_{\text{peri}} \int_{\text{peri}} D_{\text{layer}}^{k,n,k',n'}(s,z+Z_j) D^{*k,n,k',n'}_{\text{layer}}(s',z'+Z_{j'}) \\
&\quad \times \frac{e^{i(k-k')(z+Z_j-z'-Z_{j'})}}{N_{\text{cell}}^2} \Delta_{\text{rms}}^2 e^{-\sqrt{2}\sqrt{(s'-s)^2+(z'+Z_{j'}-z-Z_j)^2}/\lambda_c}\, ds\, ds' dz\, dz' \\
&= |V_{\mathrm{ESR}}^{n',k'} V_{\mathrm{ESR}}^{n,k}| \frac{\Delta_{\text{rms}}^2}{N_{\text{cell}}} \sum_{Z_{j-j'}} \int_{L_{\text{cell}}} \int_{L_{\text{cell}}} \int_{\text{peri}} \int_{\text{peri}} D_{\text{layer}}^{k,n,k',n'}(s,z) D^{*k,n,k',n'}_{\text{layer}}(s',z') \\
&\quad \times e^{i(k-k')(z-z')} e^{i(k-k')Z_{j-j'}} e^{-\sqrt{2}\sqrt{(s-s')^2+(z-z'+Z_{j-j'})^2}/\lambda_c}\, ds\, ds' dz\, dz'. \quad (10)
\end{aligned}$$

In the final expression of Eq. (10), the summation over $Z_{j-j'}$ ($= Z_j - Z_{j'}$) in the range $Z_{j-j'} \gg \lambda_c$ can be omitted. In this work, the summation was limited to the range $Z_{j-j'} \leqslant 10 \times \lambda_c$. The N_{cell} in the denominator of the last expression, which equals the number of wavenumber indexes k in the first Brillouin zone (e.g., $N_{\text{cell}} = (2\pi/L_{\text{cell}}) \times (L/2\pi) = 980$ in [110]-oriented NWs), is canceled by the density of states $L/2\pi$ in the integration over wavenumber in calculating scattering rates or collision terms.

In contrast to the case of bulk MOSFETs, where SRS is dominated by the electric field vertical to the surface and is important only at high carrier density, in NWs (and quantum wells) roughness-induced energy fluctuation is caused not only by the vertical field but also by geometrical quantum confinement [17–19]. Thus in NWs, considering both vertical field and geometrical confinement is needed to treat SRS, and SRS is important even at low carrier density. In the model described above, the effect of geometrical quantum confinement is directly included through $E_{n,k}(\delta) - E_{n,k}(0)$. By calculating $E_{n,k}(\delta) - E_{n,k}(0)$ using the electrostatic potential obtained from self-consistent calculation, the effect of the vertical field can also be considered in this model. At the same time, the two-dimensionality of the surface roughness (in other words, the existence of roughness along the confinement direction) is retained in this model.

B. Calculation procedure of hole mobility

In this subsection, the procedure to calculate the hole mobility limited by phonon scattering and SRS is described. The valence band structures and hole states of Ge NWs were computed by a nearest-neighbor $sp^3d^5s^*$ tight-binding approximation [44–47] taking the spin-orbit coupling into account. This model considers one s orbital, three p orbitals $\{p_x, p_y, p_z\}$, five d orbitals $\{d_{yz}, d_{zx}, d_{xy}, d_{3z^2-r^2}, d_{x^2-y^2}\}$, and one excited s^* orbital. For each orbital, up-spin and down-spin states are considered. Adopted tight-binding parameters were those fitted to the band structure of bulk Ge [47], and are given in Tables I and II in Ref. [47]. Surface dangling bonds were passivated by giving an excess energy to the corresponding sp^3 hybridized orbitals [42], which brings a situation similar to hydrogen termination.

To model phonon scattering atomistically [36,39], the dispersion relations and vibrational modes of phonons were calculated by a valence force field model [48–50]. Used parameters were fitted to the phonon dispersion relation of bulk Ge [49], and a free boundary condition was assumed at the surface. To calculate the scattering probability, initial and final hole states and phonon states that satisfy the wavenumber and energy conservation laws were searched using the computed valence band structure and phonon dispersion relation. Then, the transition probability was calculated for these states by Fermi's golden rule using the computed wave functions and phonon modes. All phonons were considered as inelastic scattering, and energy conservation was treated using the transformation of the delta function in Ref. [36]. The hole-phonon interaction Hamiltonian was derived from the change of the tight-binding Hamiltonian by atomic displacement due to phonons, and the matrix elements were obtained from the first-order derivative with respect to the bond vector [36,39].

The SRS rate is calculated from the model discussed in Sec. II A based on the tight-binding framework. Using the average squared matrix element [Eq. (10)] of the perturbation corresponding to surface roughness, the scattering probability was computed by Fermi's golden rule similarly to phonon scattering. The correlation length λ_c and RMS Δ_{rms} of surface roughness were assumed to be 1.3 nm and 0.48 nm, respectively [43], which are typical values used in simulations of SRS in silicon MOSFETs [19,29]. The RMS and correlation length will be different in Ge NW MOSFETs, but it was confirmed that the qualitative trends discussed below were common to the cases with doubled or halved values of RMS or correlation length.

Using the scattering probabilities calculated as above, the low-field hole mobility was computed by solving the linearized Boltzmann transport equation [36,39]. The temperature was assumed to be 300 K, and the targeted NWs were assumed to be undoped. Here, both the mobility at low hole density with the Fermi level at the mid-gap and the hole density dependence of mobility were calculated. As for the hole density dependence, hole mobility considering self-consistent calculation of band structure and potential distribution was also computed. In this case, a gate-all-around structure with metal gate and 0.6-nm-thick SiO_2 as a gate oxide were assumed.

III. RESULTS AND DISCUSSION

In this section, we discuss the calculated results of hole mobility in rectangular cross-sectional Ge NWs. Hole mobilities at low and high hole densities are shown, and their behavior is discussed in terms of hole states and valence band structures. Also, the NW geometries suitable for p-channel material in terms of hole mobility are proposed.

A. Hole mobility in germanium nanowires at low hole density

We first calculated the hole mobility at low hole density in rectangular cross-sectional Ge NWs with various orientations and substrate faces. The NW width was fixed at 4 nm, and the height was varied from 2 to 10 nm. In the model of this work, the mobility is independent of hole density as far as the hole density is low enough for the hole distribution function to be approximated by a Boltzmann distribution (hole occupation $\ll 1$). Thus, the Fermi level is fixed at the mid-gap of bulk Ge for all the NWs. In this case, owing to the negligible space charge density, the electrostatic potential in the cross section of the NWs is almost constant, and the band structure was calculated with a flat electrostatic potential. SRS thus originates from quantum confinement.

As examples to clarify the calculation process, the calculated valence band structure and scattering rates in a [110]/(001) NW with 4 nm width and 8 nm height are presented in Figs. 2(a) and 2(b), respectively. The computation of the band structure, phonon scattering, and SRS took about 1 h, 2 h, and 45 min, respectively, on our personal computer with a six-core CPU. The dashed line in Fig. 2(a) is the energy dispersion $E_{n,k}(\delta)$ used to calculate $V_{\text{ESR}}^{n,k}$ for the roughness on sidewalls. The energy variation due to sidewall displacement is larger for subbands with higher order. This causes the larger scattering rates by SRS at higher hole energy as shown in

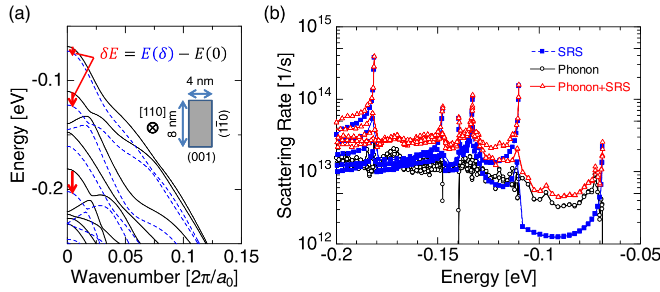

FIG. 2. (a) Valence band structure of the [110]/(001) NW with 4 nm width and 8 nm height. Dashed lines show the valence band structure when the width is reduced by two monolayers. a_0 is the lattice constant of bulk Ge (0.565 79 nm [51,52]), and the energy is referenced from the valence band maximum of bulk Ge. (b) Scattering rates by SRS, phonon scattering, and the sum of them in the same NW as (a). The peaks of scattering rates correspond to the subband edges with large DOS. The scattering rates by SRS become larger at higher hole energy (negative energy with large absolute value), because the energy variation of subbands caused by the NW width reduction is larger at higher energy.

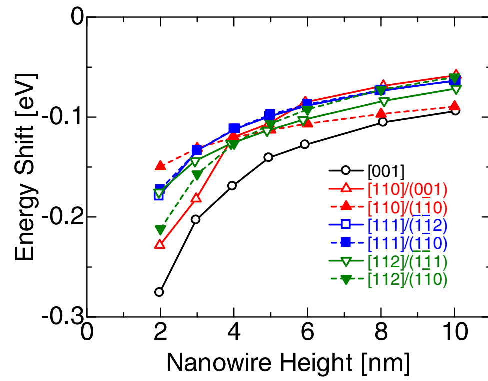

FIG. 4. The calculated confinement-induced energy shift at $k = 0$. The energy is referenced from the valence band maximum of bulk Ge. A large absolute value of energy shift means light confinement mass and gives large perturbation due to roughness.

Fig. 2(b). The peaks of scattering rates in Fig. 2(b) correspond to the subband edges with large density of states (DOS). The peaks are not so evident for the rates of phonon scattering, because of the inelastic nature of phonon scattering.

In Fig. 3(a), the height dependence of the mobility limited by both phonon scattering and SRS in Ge NWs is shown. The comparison with phonon-limited mobility is also presented for some NWs in Fig. 3(b). The phonon-limited mobility of square NWs in Fig. 3(b) is similar to the calculation in Ref. [15]. Our somewhat lower mobility in [110] and [111] NWs can be explained by the difference of cross-sectional geometry (square in the present work and circular in Ref. [15]). From Fig. 3, we can see that NWs with small cross section show low mobility with SRS. In thin NWs, where the holes are strongly confined, the quantum-confinement-induced energy of holes and its fluctuation are large. This leads to the strong SRS in thin NWs, as already reported [19,32]. The calculated confinement-induced energy shift of the first subband at $k = 0$ is shown in Fig. 4. The larger energy shift in thinner NWs can be confirmed. In some previous works on Si NWs [20,53], in contrast to the above result, stronger impacts of SRS in thicker NWs were observed due to inter-subband coupling. As can be seen from Fig. 2(b), inter-subband SRS increases the scattering rate also in the present work on Ge NWs. Since the subband separation is larger in Ge NWs than in Si NWs (for example, the separation just below the valence band maximum is 41 meV in a 4 nm × 8 nm [110]/(001) Ge NW, which is about twice as large as 19 meV in a 4 nm × 8 nm [110]/(001) Si NW), this larger subband separation in Ge NWs may weaken the impacts of inter-subband SRS on mobility in the considered cross-sectional size range and lead to the different tendency.

As for the choice of NW geometry preferable for p-channel material, the [111] NW showed the highest mobility, followed by [110], [112], and [001] NWs in descending order in the case of square cross-sectional NWs [Fig. 3(a)]. High hole mobility in [111] NWs coincides with previous reports for Si NWs [32,37,40]. In the case of rectangular cross sections, [110] NWs with the larger side (height or width) along [001] outperformed [111] NWs, owing to the highly anisotropic quantum confinement effects on holes in [110] NWs, which have been reported for Si NWs [53–55]. These results at low hole density were common to both cases with and without

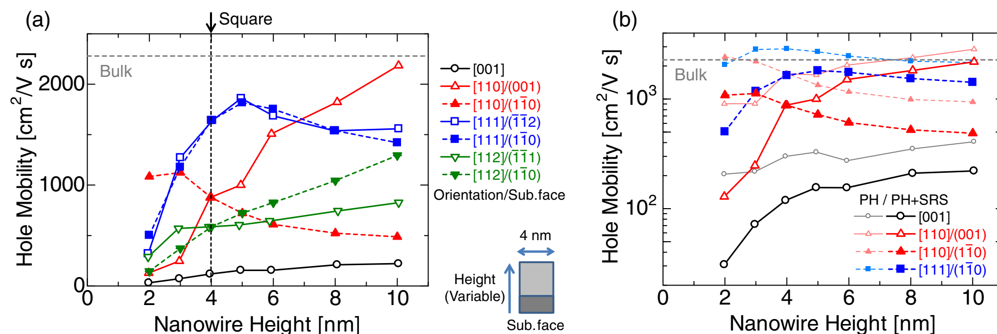

FIG. 3. (a) Height dependence of calculated hole mobility in 4-nm-wide Ge NWs with various orientations and substrate faces considering phonon scattering and SRS. The gray horizontal dashed line indicates the phonon-limited hole mobility in bulk Ge calculated by a similar method [15]. Here, the Fermi level is fixed at the mid-gap and electrostatic potential is assumed to be constant in a NW cross section. (b) The comparison between phonon-limited mobility (PH) and mobility limited by both phonon and SRS [PH+SRS, the same as (a)] for some NWs. Phonon-limited mobility is plotted by pale colored lines.

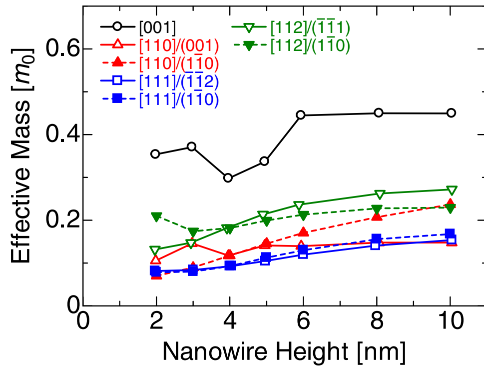

FIG. 5. The calculated hole transport mass averaged by hole distribution function. m_0 is defined as the rest mass of an electron. NWs with light transport mass tend to have heavy confinement mass, which leads to a small confinement-induced energy shift (Fig. 4).

SRS. The effective mass along the transport direction averaged by the hole distribution function is plotted in Fig. 5. This average effective mass m_{avg} was calculated as the reciprocal number of inverse effective mass averaged by equilibrium hole occupation $f_n(k)$ [16]:

$$\frac{1}{m_{\mathrm{avg}}} = \frac{\sum_n \int \frac{1}{-m_n(k)} f_n(k) dk}{\sum_n \int f_n(k) dk}. \tag{11}$$

Here, $m_n(k)$ is the effective mass at a given (n,k) as an electron. From Fig. 5, it is confirmed that NWs with high mobility have light transport mass. At the same time, smaller DOS near the band edge leads to higher mobility in both cases with and without SRS. Therefore, it seems natural that NWs with high phonon-limited mobility tend to show high mobility even with SRS. In Fig. 3(b), however, the impact of SRS, i.e., the degradation rate of mobility due to SRS, is also small in the geometries with high phonon-limited mobility. This is not so self-evident, and will be discussed in the next subsection.

In the rest of this subsection, we briefly discuss the comparison with thinner NWs with a 2 nm width. The high mobility in rectangular [110]/(001) NWs with large height and square [111] NWs was also obtained for phonon-limited hole mobility in 2-nm-wide Ge NWs [16]. However, when it comes to the comparison of mobility limited by phonon scattering and SRS ($\mu_{\mathrm{PH+SRS}}$) between NWs with 2 nm width and 4 nm width, competition between the reduction of transport mass and the enhancement of SRS both resulting from stronger quantum confinement becomes a delicate problem. Here, we focus on [110]/(001) NWs. In our previous work [16], the phonon-limited mobility in [110]/(001) Ge NWs with large height and 2 nm width (e.g., $\simeq$4000 cm^2/V s for a 2 nm × 8 nm NW) was higher than that in 4-nm-wide NWs targeted in this work. Although [110]/(001) NWs with a 2 nm width had a lighter average transport mass (e.g., $\simeq$0.07 m_0 for a 2 nm × 8 nm NW), they suffer from stronger SRS due to stronger quantum confinement. We also calculated $\mu_{\mathrm{PH+SRS}}$ of such NWs, and they showed lower mobility (e.g., $\mu_{\mathrm{PH+SRS}} \simeq 1500$ cm^2/V s for a 2 nm × 8 nm NW) than those with a 4 nm width. Of course, if the RMS of roughness is smaller, 2-nm-wide NWs may outperform 4-nm-wide NWs. For example, in case of halved RMS ($\Delta_{\mathrm{rms}} = 0.24$ nm), $\mu_{\mathrm{PH+SRS}} \simeq 2700$ cm^2/V s and $\simeq$2100 cm^2/V s for 2 nm × 8 nm and 4 nm × 8 nm NWs, respectively.

B. Relationship between the impacts of surface roughness scattering and phonon-limited mobility

In the previous subsection, by comparing both mobilities with and without SRS at each height in Fig. 3(b), we found that NWs with high phonon-limited mobility tend to be less affected by SRS. Here, we discuss the physical understanding of this aforementioned tendency about hole mobility at low hole density. As shown in Fig. 4, the confinement-induced energy shift is dependent on NW orientations and substrate faces. The larger energy shift of the hole states means high sensitivity to confinement, i.e., a light "confinement effective mass." Thus it is reasonable to interpret that the NWs with light confinement mass suffer from larger energy fluctuation by roughness and are affected by the resulting stronger SRS. This is confirmed from Fig. 4 and the degradation rate of mobility due to SRS in Fig. 3(b). If this confinement mass is heavy, the energy fluctuation is small, and thus SRS becomes weak.

On the other hand, the comparison of energy shift (Fig. 4) and transport mass (Fig. 5) tells us that the NWs with smaller energy shift, which means heavier confinement mass, tend to possess lighter transport mass, and vice versa. This negative correlation between the transport mass and confinement mass is the reason for the tendency that NWs with high phonon-limited mobility (light transport mass) are tolerant to SRS (heavy confinement mass).

To understand the physical background of the correlation of transport and confinement masses, a relationship between effective mass and wave function of holes in NWs [55] is useful. If the hole states of a subband have dominant composition of p orbitals along the transport direction, which can easily travel along the transport direction, this subband will have light transport mass and heavy confinement mass. When such subbands dominate the hole transport in a NW, the NW will have light average transport mass, which leads to high phonon-limited mobility, and heavy confinement mass, which leads to small confinement-induced energy (this itself makes it easy for the subbands to dominate transport at low density) and weak SRS. In contrast, hole states with larger composition of p orbitals along confinement directions have heavy transport mass and light confinement mass, and their contribution to conduction in a NW leads to heavier average transport mass and stronger SRS. This mechanism can explain the negative correlation between the transport mass and confinement mass, and the resulting trend of immunity to SRS of NWs with high phonon-limited mobility.

To be precise, although holes in NWs are actually confined along two directions (width and height directions), the anisotropy of confinement mass, which is evident in [110] NWs, is not considered explicitly in the discussion above. In NWs with a high aspect ratio, SRS is dominated by the confinement mass along the one direction with stronger confinement (shorter side), and thus the correlation between transport mass and SRS may not be so valid. However, as for the NWs targeted in this work (aspect ratio ∼2), the

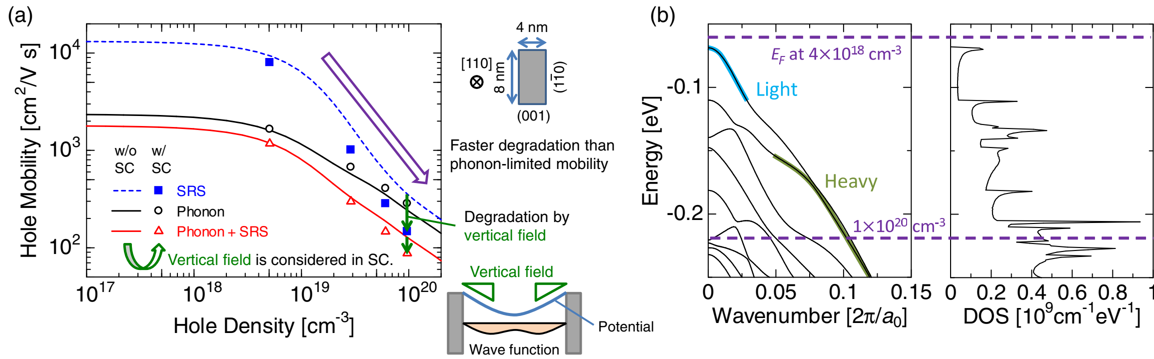

FIG. 6. (a) Hole density dependence of calculated hole mobility in a [110]/(001) Ge NW with 4 nm width and 8 nm height. Lines and symbols show the results without and with self-consistent (SC) calculation, respectively. In the case with SC, gate-all-around structure with metal gate and 0.6-nm-thick SiO_2 as a gate oxide were assumed. Steeper mobility degradation by SRS compared with phonon scattering at high hole density originates from the contribution of higher-order subbands with larger confinement energy and the vertical field. (b) The valence band structure and the DOS in the NW without SC. The Fermi level is also shown for two hole densities by horizontal dashed lines.

correspondence between light transport mass and weak SRS seems reasonable.

C. Hole density dependence of hole mobility in germanium nanowires

Here, hole density dependence of mobility is discussed. We first targeted 4 nm × 8 nm [110]/(001) Ge NW, and the calculated hole density dependence of mobility is shown in Fig. 6. The mobilities limited by SRS, phonon, and both phonon and SRS are plotted. Self-consistent (SC) calculation of the band structure and the electrostatic potential was also performed. Since the contribution of roughness-induced Coulomb-related scattering and the dielectric screening effects are not taken into account in this calculation, the mobility at high hole density may be quantitatively inaccurate, but qualitative physical trends will be maintained.

In this NW, SRS at low hole density was weak, as discussed above. At high hole density, the degradation of mobility is steeper for SRS-limited mobility than for phonon-limited mobility. As hole density increases, the Fermi level goes down, and the contribution of subbands with a heavier transport mass and larger DOS near the Fermi level [Fig. 6(b)] cause mobility degradation irrespectively of considered scattering mechanisms. In addition, SRS is enhanced at larger hole energy [Fig. 2(b)] by the larger energy fluctuation of higher-order subbands due to roughness [Fig. 2(a)]. At the same time, the effect of vertical field, which is taken into account by self-consistent calculation, on SRS becomes significant and further degrades mobility at high hole density. These factors cause steeper degradation of SRS-limited mobility than phonon-limited mobility. For these reasons, in [110]/(001) NWs, SRS is weak at low hole density, but becomes strong at high hole density.

In a previous work on cylindrical Si NWs with 12 nm diameter [34], hole mobility enhancement owing to gate-bias-induced effective mass reduction was reported. In Fig. 6(a), the slight improvement of phonon-limited mobility by SC has the same origin. However, the smaller cross-sectional size in the present work (4 nm × 8 nm) leads to light effective mass even without gate bias, and hinders the gate-bias-induced mobility enhancement.

Finally, we discuss comparison of mobility with other geometries at high hole density. The mobility limited by both phonon and SRS is compared among NWs with different orientations and substrate faces in Fig. 7. The cross section of NWs was fixed at 4 nm × 8 nm, and the results with SC are indicated by symbols. For comparison, the mobilities of some NWs calculated without SC are also shown by lines.

As can be seen from Fig. 7, the geometry dependence of mobility is small at high hole density, compared to the large geometry dependence at low hole density [Fig. 3(a)]. One reason for this is the effect of vertical field, which is less dependent on geometry than confinement mass, though this explanation only applies to the case with SC. In addition, in both cases with and without SC, the contribution of many subbands to hole transport at high hole density leads to the averaging of characteristics (confinement and transport masses) of subbands, and the difference of DOS among

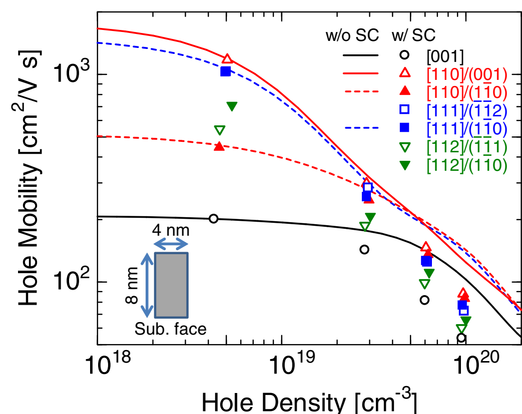

FIG. 7. Comparison of hole density dependence of hole mobility in Ge NWs with 4 nm width and 8 nm height among various geometries. Both phonon and SRS are considered, and lines and symbols show the results without and with self-consistent (SC) calculation, respectively.

different geometries is partly canceled due to the deeper degeneracy in NWs with smaller DOS. The smaller geometry dependence at high hole density has been also observed in Si NWs [33].

Though the geometry dependence of mobility is smaller at high hole density, [110] and [111] NWs still show higher mobility than other geometries. Thus, it can be concluded that these geometries are preferable as a high-mobility p-channel material even with SRS. It is interesting that the [110]/$(1\bar{1}0)$ NW exhibits high mobility at high hole density. This NW has heavier average transport mass and lower mobility at low hole density than [110]/(001) NW, which is characterized by the light mass at the band edge [Fig. 6(b)]. At high hole density, however, the average transport masses of [110]/$(1\bar{1}0)$ NW and [110]/(001) NW become comparable, owing to the contribution of hole states with higher hole energy. Thus at high hole density, the superiority of [110]/(001) NW over [110]/$(1\bar{1}0)$ NW is lost, and both types of [110] NWs exhibit similar mobility.

IV. CONCLUSION

In this work, SRS in NWs was formulated based on tight-binding approximation. By the calculated wave function of electronic states and subband energy change due to width or height fluctuation, the effect of surface roughness was expressed using an equivalent potential near the surface. The perturbation caused by a surface roughness and resulting scattering probability were computed using the equivalent potential. Then, we calculated the hole mobility in rectangular cross-sectional Ge NWs taking into account phonon scattering and SRS, and the impacts of SRS on hole mobility were analyzed. SRS at low hole density was dominated by quantum confinement, and strongly dependent on NW geometry. Because of the relationship between transport mass and confinement mass, NWs with high phonon-limited mobility tend to show high mobility even with SRS. On the other hand, at high hole density, the vertical field is important as in planer MOSFETs. In addition, the contribution of many subbands blurs the characteristics of the band edge. Thus the impacts of SRS were less dependent on NW geometry. Finally, from the geometry dependence of calculated hole mobility limited by phonon and surface roughness, we suggest that [110] Ge NWs with large height along the [001] direction and [111] Ge NWs are promising for a p-channel material.

ACKNOWLEDGMENT

This work was supported by the Japan Society for the Promotion of Science (JSPS) KAKENHI Grant No. 15J03785.

[1] S. Miyano, M. Hirose, and F. Masuoka, IEEE Trans. Electron Devices **39**, 1876 (1992).

[2] T. Saito, T. Saraya, T. Inukai, H. Majima, T. Nagumo, and T. Hiramoto, IEICE Trans. Electronics **E85-C**, 1073 (2002).

[3] J. Park and J. Colinge, IEEE Trans. Electron Devices **49**, 2222 (2002).

[4] N. Singh, A. Agarwal, L. Bera, T. Liow, R. Yang, S. Rustagi, C. Tung, R. Kumar, G. Lo, N. Balasubramanian, and D.-L. Kwong, IEEE Electron Device Lett. **27**, 383 (2006).

[5] R. Zhang, P.-C. Huang, J.-C. Lin, N. Taoka, M. Takenaka, and S. Takagi, IEEE Trans. Electron Devices **60**, 927 (2013).

[6] C. Lee, C. Lu, T. Nishimura, K. Nagashio, and A. Toriumi, in *2014 Symposium on VLSI Technology, Digest of Technical Papers, Honolulu* (IEEE, Piscataway, NJ, 2014), p. 144.

[7] J. Wang, A. Rahman, G. Klimeck, and M. Lundstrom, in *Technical Digest of the IEEE International Electron Devices Meeting, 2005, Washington, DC* (IEEE, Piscataway, NJ, 2005), p. 530.

[8] H. Minari and N. Mori, Jpn. J. Appl. Phys. **49**, 04DN04 (2010).

[9] C. S. Koong, G. Samudra, and G. Liang, Jpn. J. Appl. Phys. **49**, 04DN07 (2010).

[10] S. Mori, N. Morioka, J. Suda, and T. Kimoto, IEEE Trans. Electron Devices **60**, 944 (2013).

[11] H. Tanaka, S. Mori, N. Morioka, J. Suda, and T. Kimoto, IEEE Trans. Electron Devices **61**, 1993 (2014).

[12] D. Wang, Q. Wang, A. Javey, R. Tu, H. Dai, H. Kim, P. C. McIntyre, T. Krishnamohan, and K. C. Saraswat, Appl. Phys. Lett. **83**, 2432 (2003).

[13] J. W. Peng, N. Singh, G. Q. Lo, M. Bosman, C. Ng, and S. Lee, IEEE Trans. Electron Devices **58**, 74 (2011).

[14] R. Cheng, B. Liu, P. Guo, Y. Yang, Q. Zhou, X. Gong, Y. Dong, Y. Tong, K. Bourdelle, N. Daval, D. Delprat, B.-Y. Nguyen, E. Augendre, and Y.-C. Yeo, in *Technical Digest of the IEEE International Electron Devices Meeting, 2013, Washington, DC* (IEEE, Piscataway, NJ, 2013), p. 653.

[15] Y.-M. Niquet and C. Delerue, J. Appl. Phys. **112**, 084301 (2012).

[16] H. Tanaka, S. Mori, N. Morioka, J. Suda, and T. Kimoto, J. Appl. Phys. **116**, 235701 (2014).

[17] K. Uchida and S. Takagi, Appl. Phys. Lett. **82**, 2916 (2003).

[18] D. Esseni, IEEE Trans. Electron Devices **51**, 394 (2004).

[19] S. Jin, M. V. Fischetti, and T.-W. Tang, J. Appl. Phys. **102**, 083715 (2007).

[20] J. Wang, E. Polizzi, A. Ghosh, S. Datta, and M. Lundstrom, Appl. Phys. Lett. **87**, 043101 (2005).

[21] E. B. Ramayya, D. Vasileska, S. M. Goodnick, and I. Knezevic, J. Appl. Phys. **104**, 063711 (2008).

[22] S. Poli, M. Pala, T. Poiroux, S. Deleonibus, and G. Baccarani, IEEE Trans. Electron Devices **55**, 2968 (2008).

[23] M. V. Fischetti and S. Narayanan, J. Appl. Phys. **110**, 083713 (2011).

[24] S. Jin, M. Fischetti, and T.-W. Tang, IEEE Trans. Electron Devices **54**, 2191 (2007).

[25] T. Ando, A. B. Fowler, and F. Stern, Rev. Mod. Phys. **54**, 437 (1982).

[26] R. E. Prange and T.-W. Nee, Phys. Rev. **168**, 779 (1968).

[27] D. Pozdnyakov, Phys. Status Solidi B **247**, 134 (2010).

[28] I. M. Tienda-Luna, F. G. Ruiz, A. Godoy, B. Biel, and F. Gámiz, J. Appl. Phys. **110**, 084514 (2011).
[29] Z. Stanojević and H. Kosina, in *2013 International Conference on Simulation of Semiconductor Processes and Devices (SISPAD), Glasgow* (IEEE, Piscataway, NJ, 2013), p. 352.
[30] Z. Stanojević, O. Baumgartner, L. Filipović, H. Kosina, M. Karner, C. Kernstock, and P. Prause, Solid-State Electron. **112**, 37 (2015).
[31] Z. Stanojević, L. Filipović, O. Baumgartner, M. Karner, C. Kernstock, and H. Kosina, in *2014 15th International Conference on Ultimate Integration on Silicon (ULIS), Stockholm* (IEEE, Piscataway, NJ, 2014), p. 142.
[32] N. Neophytou and H. Kosina, Phys. Rev. B **84**, 085313 (2011).
[33] N. Neophytou and H. Kosina, Solid-State Electron. **70**, 81 (2012).
[34] N. Neophytou and H. Kosina, IEEE Electron Device Lett. **33**, 652 (2012).
[35] R. Kotlyar, T. D. Linton, R. Rios, M. D. Giles, S. M. Cea, K. J. Kuhn, M. Povolotskyi, T. Kubis, and G. Klimeck, J. Appl. Phys. **111**, 123718 (2012).
[36] W. Zhang, C. Delerue, Y.-M. Niquet, G. Allan, and E. Wang, Phys. Rev. B **82**, 115319 (2010).
[37] M. Luisier and G. Klimeck, in *Technical Digest of the IEEE International Electron Devices Meeting, 2010, San Francisco* (IEEE, Piscataway, NJ, 2010), pp. 8.6.1–8.6.4.
[38] M. Luisier, Appl. Phys. Lett. **98**, 032111 (2011).
[39] Y. Yamada, H. Tsuchiya, and M. Ogawa, J. Appl. Phys. **111**, 063720 (2012).
[40] Y.-M. Niquet, C. Delerue, D. Rideau, and B. Videau, IEEE Trans. Electron Devices **59**, 1480 (2012).
[41] Y.-M. Niquet, C. Delerue, and C. Krzeminski, Nano Lett. **12**, 3545 (2012).
[42] S. Lee, F. Oyafuso, P. von Allmen, and G. Klimeck, Phys. Rev. B **69**, 045316 (2004).
[43] S. M. Goodnick, D. K. Ferry, C. W. Wilmsen, Z. Liliental, D. Fathy, and O. L. Krivanek, Phys. Rev. B **32**, 8171 (1985).
[44] J. C. Slater and G. F. Koster, Phys. Rev. **94**, 1498 (1954).
[45] J. M. Jancu, R. Scholz, F. Beltram, and F. Bassani, Phys. Rev. B **57**, 6493 (1998).
[46] T. B. Boykin, G. Klimeck, and F. Oyafuso, Phys. Rev. B **69**, 115201 (2004).
[47] Y. M. Niquet, D. Rideau, C. Tavernier, H. Jaouen, and X. Blase, Phys. Rev. B **79**, 245201 (2009).
[48] P. N. Keating, Phys. Rev. **145**, 637 (1966).
[49] Z. Sui and I. P. Herman, Phys. Rev. B **48**, 17938 (1993).
[50] A. Paul, M. Luisier, and G. Klimeck, J. Comput. Electron. **9**, 160 (2010).
[51] J. F. C. Baker and M. Hart, Acta Crystallogr. Sect. A **31**, 364 (1975).
[52] O. Madelung, *Semiconductors: Group IV Elements and III-V Compounds* (Springer-Verlag, Berlin, 1991).
[53] N. Neophytou and H. Kosina, Appl. Phys. Lett. **99**, 092110 (2011).
[54] N. Neophytou, S. G. Kim, G. Klimeck, and H. Kosina, J. Appl. Phys. **107**, 113701 (2010).
[55] N. Morioka, H. Yoshioka, J. Suda, and T. Kimoto, J. Appl. Phys. **109**, 064318 (2011).